NEURODEVELOPMENT

Lineage-dependent spatial and functional organization of the mammalian enteric nervous system

Reena Lasrado,[1] Werend Boesmans,[1,2]* Jens Kleinjung,[1]* Carmen Pin,[3]* Donald Bell,[1] Leena Bhaw,[1]† Sarah McCallum,[1] Hui Zong,[4]‡ Liqun Luo,[4] Hans Clevers,[5] Pieter Vanden Berghe,[2] Vassilis Pachnis[1]§

The enteric nervous system (ENS) is essential for digestive function and gut homeostasis. Here we show that the amorphous neuroglia networks of the mouse ENS are composed of overlapping clonal units founded by postmigratory neural crest–derived progenitors. The spatial configuration of ENS clones depends on proliferation-driven local interactions of ENS progenitors with lineally unrelated neuroectodermal cells, the ordered colonization of the serosa-mucosa axis by clonal descendants, and gut expansion. Single-cell transcriptomics and mutagenesis analysis delineated dynamic molecular states of ENS progenitors and identified RET as a regulator of neurogenic commitment. Clonally related enteric neurons exhibit synchronous activity in response to network stimulation. Thus, lineage relationships underpin the organization of the peripheral nervous system.

Development of the nervous system and assembly of functional neural circuits depend on the proliferative expansion of neuroectodermal progenitors and the generation of neuronal and glial cell diversity. Neuronal ensembles in the brain and spinal cord are often organized according to spatial and topographic rules that ultimately dictate connectivity (*1*). In contrast, the principles governing assembly and organization of peripheral neural circuits remain obscure. The enteric nervous system (ENS) encompasses the intrinsic neural networks of the gut, which regulate gastrointestinal physiology and homeostasis (*2*). In vertebrates, the majority of enteric neurons and glia are derived from a small population of Sox10-expressing vagal neural crest cells that invade the embryonic foregut [thereafter called enteric neural crest–derived cells (ENCCs)], undergo extensive proliferation, and colonize the entire bowel (*3*). Differentiation of the expanding population of ENCCs leads to a vast mosaic of Sox10$^-$ neuronal subtypes and Sox10$^+$ glial cells, which are organized into the myenteric and the submucosal plexus (*2*, *3*). Here we provide insight into the molecular basis of cellular diversity in the ENS and demonstrate that lineage relationships underpin the spatial and functional organization of intestinal neural networks.

[1]The Francis Crick Institute, 1 Midland Road, London NW1 1AT, UK. [2]Laboratory for Enteric Neuroscience (LENS), Translational Research in GastroIntestinal Disorders (TARGID), Department of Clinical and Experimental Medicine, University of Leuven, Leuven, Belgium. [3]Institute of Food Research, Norwich NR4 7UA, UK. [4]Howard Hughes Medical Institute, Department of Biology, Stanford University, Stanford, CA 94305, USA. [5]Hubrecht Institute–KNAW (Royal Netherlands Academy of Arts and Sciences) and University Medical Centre Utrecht, 3584 CT Utrecht, Netherlands.
*These authors contributed equally to this work.
†Present address: Biomedical Research Centre Genomics Laboratory, Imperial College London, Room 4N5, Commonwealth Building, Du Cane Road, London W12 0NN, UK.
‡Present address: Department of Microbiology, Immunology, and Cancer Biology, University of Virginia School of Medicine, Charlottesville, VA 22908, USA.
§Corresponding author. Email: vassilis.pachnis@crick.ac.uk

Generation and lineage composition of ENS clones

To examine the developmental potential of individual ENS progenitors in mammals, we used Cre/LoxP technology to fate map Sox10$^+$ ENCCs in mouse embryos. Animals transgenic for the *Sox10::CreER^{T2}* (SER93) driver (*4*) and the *Rosa26EYFP* (*5*) or *Rosa26Confetti* (*6*) reporters (called SER93|EYFP or SER93|Confetti, respectively) were exposed to a single dose of tamoxifen at embryonic day 12.5 (E12.5) and analyzed 24 to 72 hours later (fig. S1). Distinct clusters of labeled cells were detected in the stomach, small intestine, and cecum of both sets of transgenic mice (fig. S1). The spatial isolation, the similar distribution and number but progressive size increase (fig. S1), and the monochromatic character (in SER93|Confetti mice) of the clusters suggested clonal origin. Using a different *Sox10::CreER^{T2}* transgene (SER26) (*4*) and the *Rosa26tdTomato* reporter (*7*) (SER26|tdT), we estimated that the 2.84-fold increase in the total ENCC number in the small intestine from E13.5 to E15.5 (see supplementary materials) matches the 2.86-fold increase in the average size of small intestine clusters during this period (fig. S1). Spatially isolated monochromatic cell clusters were also identified in the ENS of adult SER93|Confetti animals exposed to tamoxifen at E12.5 (Fig. 1, A to D). The number and distribution of clones in the adult ENS were similar to those detected during embryogenesis (fig. S1). Therefore, the vast majority of Sox10$^+$ ENCCs labeled in E12.5 SER93|Confetti embryos give rise to spatially identifiable ENS clones in adult mice.

To gain insight into the developmental potential of ENCCs at E12.5, we analyzed the cell type composition of ENS clones in adult Ser93|Confetti mice. Approximately a quarter of clones contained both neurons and glia (NG clones) (Fig. 1, B, E, and H, and fig. S2), a smaller fraction were composed exclusively of neurons (N clones) (Fig. 1, C, F, and H), and the majority included only glial cells (G clones) (Fig. 1, D, G, and H). NG and G clones were, on average, larger relative to N clones (Fig. 1H). Consistent with earlier fate-mapping studies of the mammalian neural crest (*8*–*10*), we conclude that Sox10$^+$ ENCCs include bipotential (NG) progenitors and fate-restricted gliogenic (G) precursors with high but variable proliferative potential and fate-restricted neurogenic (N) precursors with limited proliferative capacity.

NG clones (n = 15) included multiple neuronal subtypes (figs. S2 and S3A), indicating that the founder progenitors give rise to multiple classes of enteric neurons. All 8- to 16-neuron N clones (n = 5) immunostained for calretinin (CALR) and neuronal nitric oxide synthase (nNOS), which identify nonoverlapping subsets of enteric neurons in the myenteric plexus (*11*), contained combinations of CALR$^+$, nNOS$^+$, and CALR$^-$nNOS$^-$ neurons (fig. S3C and table S1). In contrast, none of the two- to four-neuron clones (n = 21) immunostained for CALR, nNOS, or neurofilament M (*11*) coexpressed these markers (fig. S3D and table S1), suggesting that enteric neuron subtype specification occurs at the penultimate or final cell division. We also found that NG and G progenitors give rise to all types of enteric glia (fig. S3B) (*12*). Therefore, our genetic labeling strategy targets a representative ENS progenitor pool in mammals.

Single-cell RNA sequencing of ENS progenitors

To identify transcriptional signatures of ENS lineage fate restriction and differentiation, we carried out single-cell RNA sequencing (scRNA-seq) of ENCCs isolated from E12.5 to 13.0 *Sox10::CreER^{T2};Rosa26tdTomato* (SER93|tdT) embryos. Principal components analysis (PCA) identified a relatively compact cluster of cells expressing markers of undifferentiated ENS progenitors or glia (*Sox10*, *Erbb3*, *Fabp7*, *Plp1*) (*13*–*15*) (Fig. 2A). This group extended into a diffuse cell population marked by expression of the neuron-specific genes *Tubb3* and *Elavl4* (Fig. 2A). *Ret* and *Phox2B*, which are activated in early ENS progenitors but maintained specifically in enteric neurons (*16*), were also associated with this neurogenic trajectory (Fig. 2A). Therefore, at E12.5 ENCCs represent two contiguous but diverging cellular states defined by progenitor/gliogenic (*Erbb3*, *Sox10*, *Fabp7*, and *Plp1*) or progenitor/neurogenic (*Tubb3*, *Elavl4*, *Ret*, and *Phox2b*) marker genes.

Hierarchical clustering of ENCC transcriptomes highlighted the close relationship between *Sox10/Erbb3* and *Fabp7/Plp1* genes and subdivided the ENCC population into three clusters (Fig. 2B). Cluster 1 (C1) cells expressed the neuronal markers *Tubb3* and *Elavl4* (but were negative for the progenitor/gliogenic module) (Fig. 2, B and C),

were located along the neurogenic trajectory (small orange cells in Fig. 2A), and were mostly noncycling, which suggests that they represent relatively advanced stages of neuronal differentiation. The C2 cluster was further subdivided into C2a cells, which coexpressed the progenitor/neurogenic and progenitor/gliogenic modules, and C2b cells, which expressed the progenitor/gliogenic markers but were generally negative for *Tubb3* and *Elavl4* (Fig. 2, B and C). The "mixed identity" and broad distribution of C2a cells across divergent cellular states (large magenta circles in Fig. 2A) suggested that they correspond to an early transient stage of the neurogenic lineage and that, together with C1 cells, they represent distinct stages of N precursor trajectory. The remaining cell population of the C2 cluster (C2b) is likely to include uncommitted (NG) progenitors and glia-committed (G) precursors (Fig. 2, B and C). The further subdivision of the C2b subgroup into Ret^{high} and Ret^{low} subpopulations and the down-regulation of *Ret* in enteric glia (*17*) suggest that the transcriptomes of uncommitted (NG) progenitors and glia-committed (G) precursors can be distinguished at this stage by expression of *Ret* and that this gene plays a pivotal role in the decision of undifferentiated ENS progenitors to follow the neurogenic fate. Our analysis also identified a small cell cluster (C3) that expressed low levels of all markers used (Fig. 2, B and C). Next we evaluated gene correlation by linear regression analysis against the marker genes *Tubb3* and *Erbb3*, whose vectors define the main axis of PCA plot variation (Fig. 2A). Identified genes encode neuron-specific components of the ENS (*Chrna3*, *Chrnb4*, *Gap43*, *Scg3*, *Syt4*) (*18*) or have been implicated in ENS development (*Nid1*) (*19*), neurogenesis (*Heyl*) (*20*), or gliogenesis (*Nfia*) (*21*) (Fig. 2D). Therefore, our single-cell transcriptomic studies provide a molecular view of ENCC dynamics at a critical period of ENS histogenesis and identify potential regulators of enteric neurogenesis and gliogenesis.

RET signaling controls neurogenic fate restriction

The dynamics of ENCC expansion and the role of *Ret* in ENS lineage development were further analyzed by mosaic analysis with double markers (MADM). Combination of *MADM6-GR* and *MADM6-RG* alleles (*22*) with the *Sox10::Cre* transgene (*23*) (Sox10Cre|MADM mice) (fig. S4) resulted in green fluorescent protein (GFP)– and red fluorescent protein (RFP)–labeled twin cell clusters from E12.5 to E13.5 (Fig. 3A). The total GFP^+ and RFP^+ cell populations in the gut of E16.5 and postnatal day 5 (P5) animals were similar (fig. S4). In addition, pairwise comparison of GFP- and RFP-labeled sister clusters at E16.5 showed that they had similar sizes (Fig. 3B). Together, these findings suggest equivalent proliferative potential of the twin cluster founder cells and a predominantly symmetric mode of cell division and confirm the low levels of ENS cell death during development (*24*).

The telomeric location of *Ret* relative to the *Rosa26* (MADM) locus (www.ensembl.org)

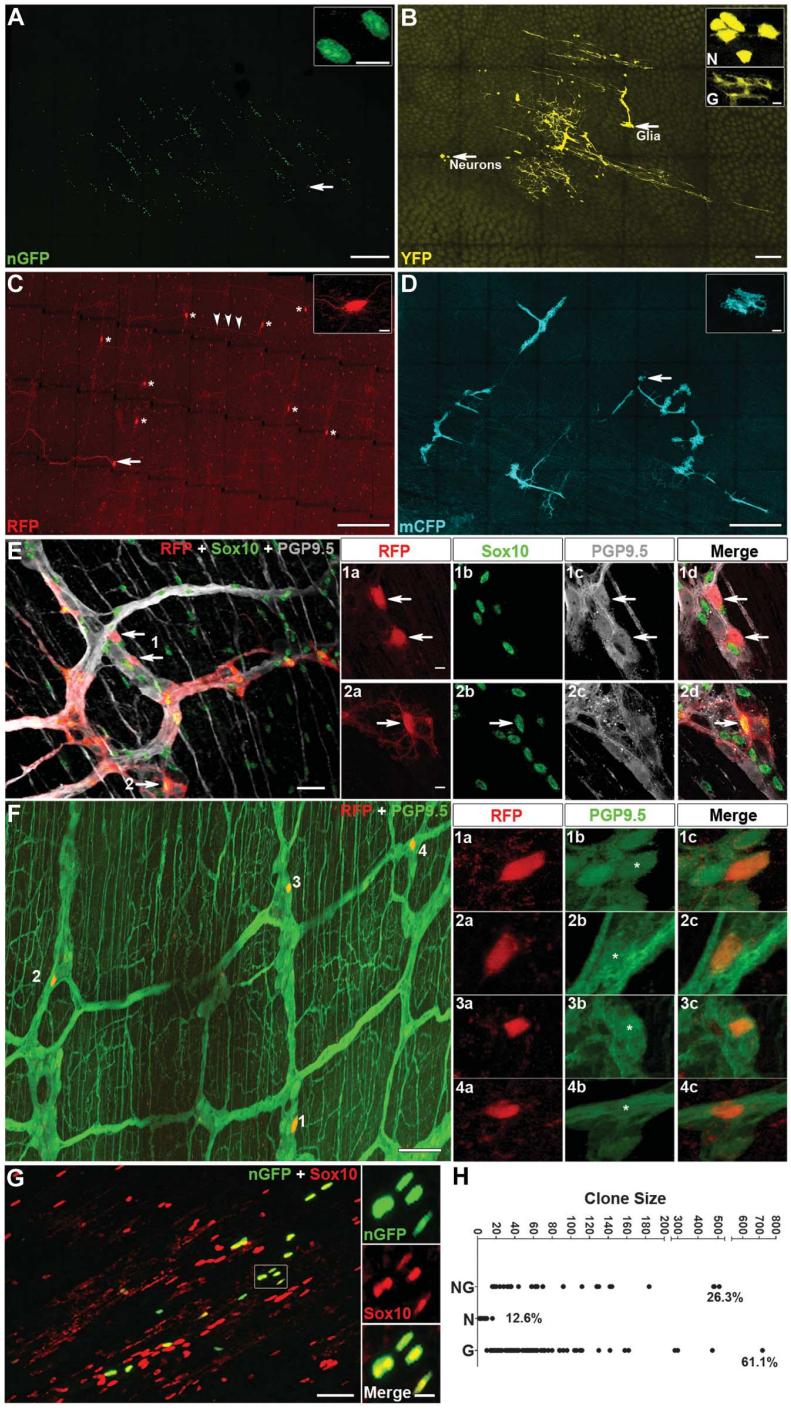

Fig. 1. Lineage composition of adult enteric nervous system (ENS) clones. (**A** to **D**) Monochromatic ENS clones in adult SER93|Confetti mice expressing nuclear GFP (nGFP) (A), YFP (B), RFP (C), and membrane CFP (mCFP) (D). Insets show magnifications of cells indicated by arrows in the corresponding panels. The YFP^+ clone contains neurons (N) and glia (G). The RFP^+ clone includes only neurons (indicated by asterisks); arrowheads indicate neuronal projections. The mCFP clone contains only glia. Scale bars: main panels, 500 μm; insets, 5 μm (A), 10 μm [(B) and (C)], 20 μm (D). (**E**) RFP^+ clone immunostained for Sox10 (glia) and PGP9.5 (neurons). Panels 1a to 1d and 2a to 2d show magnifications of RFP^+ cells indicated by arrow sets 1 and 2, respectively. This clone contains both neurons and glia. Scale bars: main panel, 200 μm; 1a to 2d, 10 μm. (**F**) RFP^+ clone immunostained for PGP9.5. Panels 1a to 1c, 2a to 2c, 3a to 3c, and 4a to 4c show magnifications of the area around cells 1 to 4. All RFP^+ cells are neurons. Scale bars: main panel, 200 μm; 1a to 4c, 10 μm. (**G**) $nGFP^+$ clone immunostained for Sox10 (glia). Insets show magnifications of the boxed area. Scale bars: main panel, 200 μm; insets, 5 μm. (**H**) Size distribution and percentage of NG, N, and G clones.

allowed us to link the Ret^{k-} null allele (*25*) to the MADM-GR cassette (*MADM6-GR-Ret*$^{k-}$ allele) (fig. S4). *Sox10::Cre*-mediated recombination in *MADM6-GR-RET*$^{k-}$/*MADM6-RG* embryos (Sox10Cre|MADM-Ret^{k-}) generated Ret-deficient GFP$^+$ and wild-type RFP$^+$ clusters similar to those observed in Sox10Cre|MADM animals (Fig. 3C and fig. S4). Despite the prosurvival role of RET in early ENS progenitors (*26*), the total number of Ret-deficient GFP$^+$ cells was significantly higher relative to the RFP$^+$ cell population (fig. S4) and at E16.5 the majority of GFP$^+$ clusters were larger relative to their RFP$^+$ sisters (Fig. 3D), suggesting that clonal deletion of *Ret* in E12.5 ENCCs confers growth advantage in a cell-autonomous manner. Finally, the representation of neurons within the GFP$^+$ (Ret-deficient) cell population of Sox10Cre|MADM-Ret^{k-} guts relative to their RFP$^+$ counterparts (wild type) was reduced at E16.5 and P5 (fig. S4), supporting a role of RET signaling in neurogenic commitment of bipotential ENS progenitors.

Topological organization of ENS clones

Next we examined the spatial organization of ENS clones in adult SER93|Confetti mice induced by tamoxifen at E12.5. All clones occupied well-defined domains of the myenteric plexus (Fig. 1, A to D), indicating that long-range migration is not implicated in the distribution of ENCC descendants within this layer. The relationship between clone size and surface area for all types of clones (fig. S5) suggested that clonal spread within the myenteric plexus depends on the proliferative potential of the founder cells. Next, we considered the effect of cell division on short-range interactions between ENCC descendants and lineally unrelated neuroectodermal neighbors by devising an agent-based computational model that simulates virtual cells on a two-dimensional (2D) lattice over time (*27*) (see supplementary materials and movie S1). Simulation of clonal expansion within a growing unlabeled cell population resulted in larger spread relative to clones growing in isolation and different-size clones spreading over similar area (fig. S5 and movies S1 to S3), suggesting that proliferation-driven interactions between labeled and nonlabeled ENCCs influence the spatial organization of clones. The computational model predicts that clones originating from neighboring founder cells occupy overlapping domains (fig. S5 and movie S4). Overlapping ENS clones were observed in the gut of SER93|Confetti mice exposed at E12.5 to a fourfold higher dose of tamoxifen (Fig. 4A). We conclude that the myenteric plexus is assembled from overlapping clonal units of ENCCs (Fig. 4D).

To further explore the factors that contribute to the spatial organization of ENS clones, we developed an analytical model for ENS clone size and tested it against independent experimental measurements (supplementary text). Although the values generated from this model were substantially smaller in comparison to the experimental ones, introduction of a term describing isometric increase of clonal spread during gut development resulted in estimates that were in good agreement with observations (fig. S5 and supplementary text). Therefore, during gut organogenesis, clonally related ENS cells are displaced in a scaling manner without altering the relative arrangement of clones in space. Together, experiments and modeling indicate that the myenteric plexus is composed of overlapping clonal units whose size depends on the intrinsic properties of the founder progenitors, interactions of descendants with lineally unrelated neuroectodermal neighbors, and organogenesis-associated physical changes of the gut.

Next we examined the distribution of clonally related ENS cells along the serosa-mucosa axis of the gut cylinder. All clones contributed to the myenteric plexus (Fig. 1), but the contribution of sister cells to the submucosal plexus and the mucosa depended on clone type. N clones were invariably restricted to the myenteric plexus (26 of 26 clones), but sister cells of NG and G clones were often found in the submucosal plexus and the mucosa (Fig. 4, B and C, and figs. S2 and S6). In NG and G clones, sister glial cells were detected in the mucosal layer only if the submucosal layer was also colonized (Fig. 4C). Therefore, during gut organogenesis, the progeny of NG and G progenitors have the potential of colonizing all layers of the ENS and appear to do so in a sequential "outside-in" manner (fig. S6). Finally, color-coding sister cells along the serosa-mucosa axis and examination of cross-section views of the gut wall demonstrated that labeled cells located within the submucosal plexus and the mucosa were in register with their sister cells in the myenteric plexus (Fig. 4, B and C). Therefore,

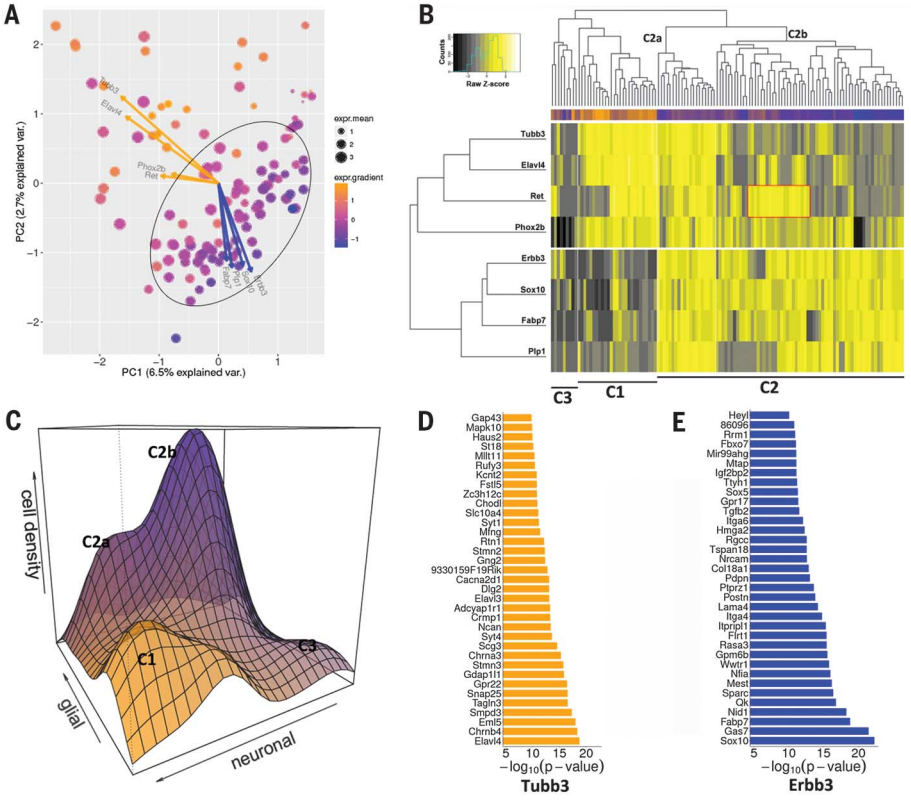

Fig. 2. Single-cell RNA sequencing identifies cell types in embryonic ENS. (**A**) PCA of 120 single-cell ENCC transcriptomes based on variable genes identified. Biplots show the variance of gene expression in single cells and the direction of marker genes (vectors) projected onto PC1 and PC2. Arrow tips indicate the correlation coefficient of the respective gene with the PCs. The gradient of gene marker expression is color coded (neuronal, orange; glial, blue), and the mean total marker gene expression is size coded on a $\log_{10}$ scale. The neurogenic lineage (mostly small orange and large magenta circles) forms a diffuse cluster emerging from the bulk of cells (mostly magenta and small blue circles within the ellipsoid) that includes bipotential progenitors and gliogenic precursors. The distribution of cells in the PCA plot and most of the gene expression variance is reflected by the *Tubb3-Erbb3* axis. (**B**) Heat map of marker gene expression (color coded in increasing order: black, gray, yellow, white). Shown are two clusters of marker genes [progenitor/neuronal (*Tubb3*, *Elavl4*, *Ret*, and *Phox2b*) and progenitor/glial (*Erbb3*, *Sox10*, *Fabp7*, and *Plp1*)] and three main cell clusters (C1 to C3). The color bar along the cell axis illustrates the expression gradient between neuronal and glial markers (neuronal, orange; glial, blue). The red box in C2b indicates high *Ret*-expressing cells. (**C**) Perspective plot of single-cell density as a function of expression levels of progenitor/neuronal (orange) and progenitor/glial (blue) markers. (**D** and **E**) Genes correlated with *Tubb3* (orange) and *Erbb3* (blue) shown as bars sorted according to log-transformed *P* values as a measure of correlation strength. *P* values are from linear regression analysis against the marker genes.

lineally related cells of NG and G clones are organized as columns along the serosa-mucosa polar axis of the gut cylinder (Fig. 4D).

Coordinate activity of clonally related enteric neurons

The clustering of clonally related enteric neurons in the adult mouse gut raised the possibility that their activities are coordinated. To examine this, live preparations of myenteric plexus from SER93|Confetti mice (induced with tamoxifen at E12.5) were loaded with the calcium indicator Fluo-4, and intracellular [Ca^{2+}] tracings of sister and lineally unrelated neurons were compared following subtle electrical stimulation of interganglionic connectives (Fig. 5, A to C, and fig. S7). Notably, more synchronous Ca^{2+} responses were detected between RFP^+ sister neuron pairs relative to the nonlabeled control cells (Fig. 5, D to F). Intraganglionic sister pairs were not different from interganglionic pairs regarding the synchronous display of Ca^{2+} responses (Fig. 5G). Furthermore, the synchronous behavior of sister pairs was independent of the targeted interganglionic nerve strand. Therefore, clonally related enteric neurons respond to activation signals in a more synchronized manner relative to their nonlineally related counterparts.

By combining progenitor fate mapping with transcriptomic analysis and activity mapping at single-cell resolution, we provide evidence that lineage relationships dictate key aspects of ENS development, organization, and function. The demonstration that individual ENS progenitors coexpress divergent transcriptional programs provides a molecular framework for understanding their considerable flexibility in cell fate choice and how signals from the local microenvironment control the stage-dependent generation of distinct lineages during the protracted period of enteric neurogenesis and gliogenesis (*4*). Activation of *Ret* in bipotential ENS progenitors is essential for neurogenic commitment and diversion from an ostensibly default glial fate that would be otherwise promoted by gliogenic factors. This view underscores the close relationship between undifferentiated ENS progenitors and glial cells (*4*) and suggests that the estimated frequency of G cells in our current studies reflects the probability of bipotential progenitors to follow the gliogenic option at a given stage rather than their irreversible commitment to the glial lineage. Further characterization of the transcriptional programs that define distinct stages of enteric neurogenesis and gliogenesis will provide imperative insight into the molecular mechanisms that control development of ENS lineages. Our studies also provide insight into the 3D organization of the ENS. We propose that the ENS of the small intestine in mammals is built from parallel and overlapping columns of clonally derived cells that extend throughout the entire width of the gut wall and are arranged along the serosa-mucosa axis (Fig. 4D). Each columnar unit is derived from a founder NG progenitor, which settles into a chosen site within the prospective myenteric plexus and generates progeny that

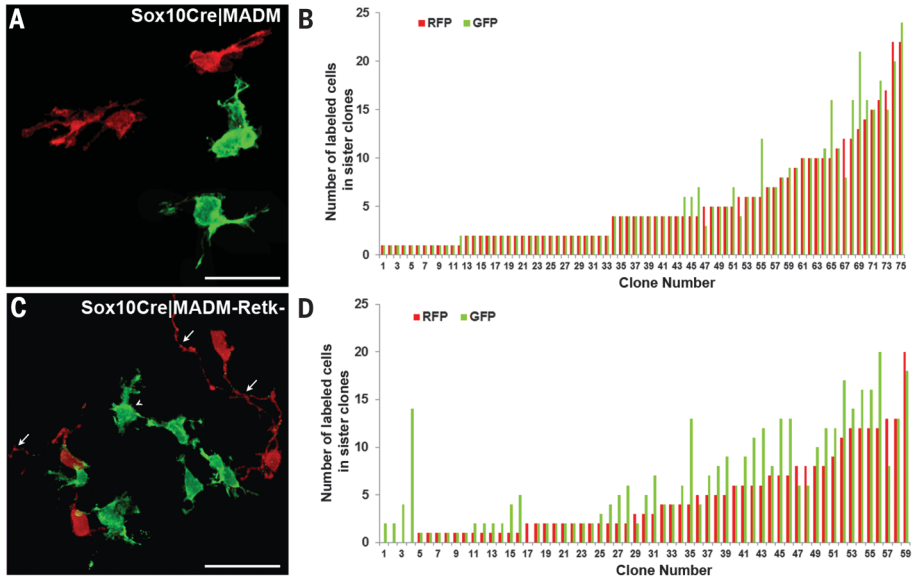

Fig. 3. Wild-type and Ret-deficient mosaic analysis with double markers (MADM) ENS clusters. (**A**) Twin GFP^+ (green) and RFP^+ (red) clusters in the gut of Sox10Cre|MADM embryos. (**B**) Pairwise comparison of sister GFP^+ and RFP^+ clusters identified in E16.5 Sox10Cre|MADM embryos. Wilcoxon signed-rank test: $P > 0.05$ ($P = 0.0847$). (**C**) Twin GFP^+ and RFP^+ clusters in Sox10Cre|MADM-Ret^{k-} embryos. Most RFP^+ cells (wild type) have obvious neuronal projections (arrows), whereas GFP^+ cells (Ret-deficient) show typical morphology of undifferentiated progenitors. (**D**) Pairwise comparison of sister GFP^+ and RFP^+ clusters identified in E16.5 Sox10Cre|MADM-Ret^{k-} embryos. Wilcoxon signed-rank test: $P < 0.05$ ($P = 0.000412$). Scale bars in (A) and (C): 50 μm.

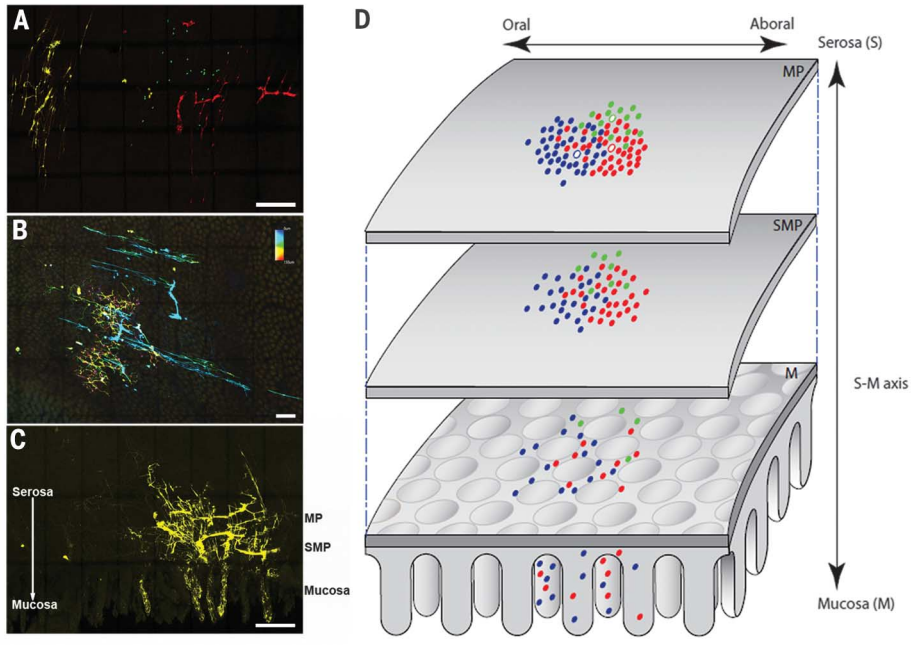

Fig. 4. Topological organization of ENS clones in adult mouse gut. (**A**) Overlapping ENS clones in adult SER93|Confetti animals exposed to tamoxifen (40 μg/g of dam body weight) at E12.5. (**B**) Color-coding for depth indicates that sister cells of single clones occupy different ENS layers. Deep cells are immediately underneath superficially located sisters. (**C**) Cross-section view of a YFP^+ clone. The vast majority of cells in the myenteric plexus (MP), submucosal plexus (SMP), and mucosa are in register along the serosa-mucosa axis. (**D**) Model depicting the organization of small intestine ENS into overlapping columns along the serosa-mucosa axis. Each clone originates from a founder cell (white) that settles in a given location within the outer gut wall (future MP) and gives rise to progeny that either remain in the vicinity or colonize in a stepwise manner the SMP and mucosa. Sister cells are in register along the serosa-mucosa axis. Scale bars in (A) to (C): 500 μm.

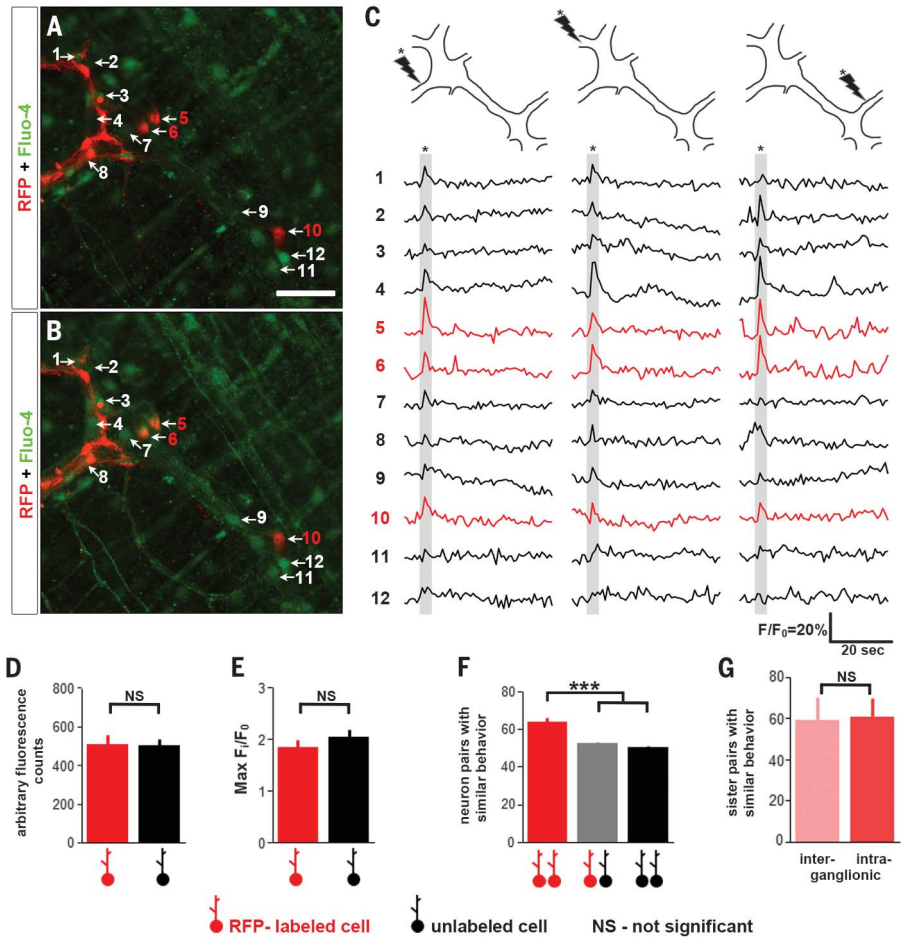

Fig. 5. Coordinate activity of sister neurons. (**A** and **B**) Fluorescence micrograph of a live preparation of myenteric plexus (including part of an RFP$^+$ clone) loaded with Fluo-4 (green) at baseline (A) or during a train of electrical pulses (300 μs, 20 Hz, 2 s) (B). Analyzed neurons are indicated by arrows. Neurons 5, 6, and 10 belong to the RFP clone, and RFP$^-$ neurons were used as lineally unrelated controls. Scale bar: 50 μm. (**C**) Fluo-4 tracings (bottom) of neurons after single-pulse electrical stimulation conveyed to three different interganglionic nerve strands (top). F, arbitrary fluorescence; F_0, F at time point 0. (**D**) Baseline intracellular Ca^{2+} levels in RFP$^+$ and RFP$^-$ neurons (two-tailed Student's *t* test, $P > 0.05$). (**E**) Maximal amplitude of Ca^{2+} transients induced by an electric pulse train in RFP$^+$ and RFP$^-$ neurons (two-tailed Student's *t* test, $P > 0.05$). (**F**) Proportion of neuronal pairs that display coordinate Ca^{2+} responses to single electrical pulses [one-way analysis of variance (ANOVA), $P < 0.0001$; Dunnett's multiple comparison test, $^{***}P < 0.001$ versus pairs of RFP-labeled sister neurons]. (**G**) Proportion of sister pairs present in the same ganglion compared to sister pairs located in different ganglia that display coordinate Ca^{2+} responses to single electrical pulses (two-tailed Student's *t* test, $P > 0.05$). Error bars in (D) to (G) indicate SEM.

either remain within its immediate vicinity or cross in a stepwise manner to form the submucosal plexus and eventually the mucosal ENS (fig. S6). Only NG- and G-type progeny have the potential to colonize the submucosal plexus and the mucosa while myenteric and submucosal neurons are generated sequentially from plexus-specified neurogenic precursors, which are restricted to the respective ganglionic layer (fig. S6). This hierarchical model integrates early stages of ENS development, dominated by enteric neuron and glia progenitor allocation in the prospective myenteric plexus, with later events relating to the organization of the ENS within the 3D space of the intestinal wall. Given the different strategies employed for the migration of ENS progenitors in the small intestine and the colon (*28*), it will be interesting to explore the underlying differences in the assembly and organization of neural networks in the two parts of the gastrointestinal tract. Our work also suggests that ontogenetic clonal units organized within columnar spaces along the gut constitute fundamental elements in the functional architecture of the ENS. It is currently unclear whether the increased propensity for synchronization of clonally related myenteric neurons is due to the preferential formation of chemical or electrical synapses or common input from lineally unrelated neurons. In addition, it remains unknown whether sister neurons located in different layers of the ENS also show increased synchronization. Despite these limitations, allocation of lineally related enteric neurons into parallel and overlapping clonal units provides an opportunity to integrate the physiological activity of neuronal ensembles along the longitudinal and radial axis of the gut and contributes to the functional integration of the ENS.

REFERENCES AND NOTES

1. Y. Tanabe, T. M. Jessell, *Science* **274**, 1115–1123 (1996).
2. J. Furness, *The Enteric Nervous System* (Blackwell, 2006).
3. M. Avetisyan, E. M. Schill, R. O. Heuckeroth, *J. Clin. Invest.* **125**, 899–907 (2015).
4. C. Laranjeira *et al.*, *J. Clin. Invest.* **121**, 3412–3424 (2011).
5. S. Srinivas *et al.*, *BMC Dev. Biol.* **1**, 4 (2001).
6. H. J. Snippert *et al.*, *Cell* **143**, 134–144 (2010).
7. L. Madisen *et al.*, *Nat. Neurosci.* **13**, 133–140 (2010).
8. A. Baggiolini *et al.*, *Cell Stem Cell* **16**, 314–322 (2015).
9. G. M. Kruger *et al.*, *Neuron* **35**, 657–669 (2002).
10. J. T. Mosher *et al.*, *Dev. Biol.* **303**, 1–15 (2007).
11. A. J. Bergner *et al.*, *J. Comp. Neurol.* **522**, 514–527 (2014).
12. W. Boesmans, R. Lasrado, P. Vanden Berghe, V. Pachnis, *Glia* **63**, 229–241 (2015).
13. H. M. Young, A. J. Bergner, T. Müller, *J. Comp. Neurol.* **456**, 1–11 (2003).
14. A. Chalazonitis, F. D'Autréaux, T. D. Pham, J. A. Kessler, M. D. Gershon, *Dev. Biol.* **350**, 64–79 (2011).
15. M. Rao *et al.*, *Glia* **63**, 2040–2057 (2015).
16. H. M. Young *et al.*, *Dev. Biol.* **202**, 67–84 (1998).
17. V. Sasselli, V. Pachnis, A. J. Burns, *Dev. Biol.* **366**, 64–73 (2012).
18. T. A. Heanue, V. Pachnis, *Proc. Natl. Acad. Sci. U.S.A.* **103**, 6919–6924 (2006).
19. D. Zhu *et al.*, *J. Neurochem.* **134**, 39–46 (2015).
20. A. Jalali *et al.*, *J. Neurosci. Res.* **89**, 299–309 (2011).
21. M. Caiazzo *et al.*, *Stem Cell Rep.* **4**, 25–36 (2015).
22. H. Zong, J. S. Espinosa, H. H. Su, M. D. Muzumdar, L. Luo, *Cell* **121**, 479–492 (2005).
23. T. Matsuoka *et al.*, *Nature* **436**, 347–355 (2005).
24. H. Enomoto, *Neurogastroenterol. Motil.* **21**, 684–687 (2009).
25. A. Schuchardt, V. D'Agati, L. Larsson-Blomberg, F. Costantini, V. Pachnis, *Nature* **367**, 380–383 (1994).
26. R. O. Heuckeroth, P. A. Lampe, E. M. Johnson Jr., J. Milbrandt, *Dev. Biol.* **200**, 116–129 (1998).
27. B. L. Cheeseman, D. Zhang, B. J. Binder, D. F. Newgreen, K. A. Landman, *J. R. Soc. Interface* **11**, 20130815 (2014).
28. A. J. Burns, N. M. Le Douarin, *Anat. Rec.* **262**, 16–28 (2001).

ACKNOWLEDGMENTS

The transcriptome sequencing data for all single cells have been deposited in the European Molecular Biology Laboratory–European Bioinformatics Institute ArrayExpress database under accession number E-MTAB-5553 (www.ebi.ac.uk/arrayexpress/experiments/E-MTAB-5553). We thank members of the Pachnis laboratory and T. Vogt for discussions and comments on the manuscript, J. Bornstein for educational discussions about ENS function, T. Margrie and D. Burdakov for lab space and advice relating to the Ca^{2+} imaging experiments, A. Sesay for advice and support with scRNA-seq, and the staff of the Biological Research Facility and the Flow Cytometry Science Technology Platform of the Crick Institute for advice and expert help. P.V.B. was supported by Fonds voor Wetenschappelijk Onderzoek (FWO-Flanders; grants G.0510.10 and G.0921.015). W.B. was a recipient of a postdoctoral fellowship from FWO-Flanders. C.P. acknowledges the support of the UK Biotechnology and Biological Sciences Research Council (BBSRC) Gut Health and Food Safety Programme Grant (BB/J004529/1). Work in V.P.'s laboratory is supported by the BBSRC (BB/L022974/1), the UK Medical Research Council (MRC), and the Francis Crick Institute (which receives funding from the MRC, Cancer Research UK, and the Wellcome Trust). The supplementary materials contain additional data.

SUPPLEMENTARY MATERIALS

www.sciencemag.org/content/356/6339/722/suppl/DC1
Materials and Methods
Supplementary Text
Figs. S1 to S7
Tables S1 and S2
References (*29*–*34*)
Movies S1 to S4

20 January 2017; accepted 10 April 2017
10.1126/science.aam7511

Lineage-dependent spatial and functional organization of the mammalian enteric nervous system

Reena Lasrado, Werend Boesmans, Jens Kleinjung, Carmen Pin, Donald Bell, Leena Bhaw, Sarah McCallum, Hui Zong, Liqun Luo, Hans Clevers, Pieter Vanden Berghe and Vassilis Pachnis

Science **356** (6339), 722-726.
DOI: 10.1126/science.aam7511

Neural crest rules the gut

The neurons and glial cells that regulate gut function derive from neural crest cells that emerge from the developing neural tube. Lasrado *et al.* used single-cell transcriptomics and mosaic mutagenesis to follow how the enteric nervous system is built in mice. Overlapping expression of regulatory programs supports dynamic determination of cell fates, with the developing neurons organized by clonal lineages. The clonal build model may explain how gut motility is coordinated in sequential segments and gut secretion is coordinated with motility.

Science, this issue p. 722